

Observations of short-circuiting flow paths within a free-surface wetland in Augusta, Georgia, U.S.A.

Anne F. Lightbody,¹ Margaret E. Avenir,² and Heidi M. Nepf

Ralph M. Parsons Laboratory, Department of Civil and Environmental Engineering, Massachusetts Institute of Technology, 77 Massachusetts Ave., Cambridge, Massachusetts 02139

Abstract

Velocity heterogeneity is characteristic of wetland systems and results in some influent water remaining in the wetland for less than the expected residence time on the basis of volume and flow rate. This phenomenon, known as short-circuiting, alters the distribution of the chemical and biological transformations that occur within the wetland. Field observations in a 1.5-km² constructed treatment wetland in Augusta, Georgia were used to quantify the size, distribution, velocity, and transport potential of fast flow paths, which cause short-circuiting within wetlands. The flow paths were identified by a tracer study and velocity measurements. In each of the three cells examined, between three and six fast flow paths were found, most less than 4 m wide. These flow paths had an area-averaged velocity on the order of 1 cm s⁻¹, at least 10 times the velocity observed where water passed through vegetation. Within different cells in this wetland, 20–70% of the flow had a residence time less than one-eighth of the nominal residence time. With this degree of short-circuiting, uniform flow is a poor approximation for the flow through the wetland. In addition, tracer studies were used to make direct measurements of mixing within open-water deep zones. Lateral mixing was sensitive to the direction of the wind. The average daily maximum temperature in the densely vegetated slow-flow zones was 2.0°C cooler than that at the surface of the open water zones and 0.9°C cooler than that of the fast-flow zones. The importance of short-circuiting flow paths in this relatively simple wetland suggests that this phenomenon is likely of even greater significance in natural wetlands because they are typically much more complex.

There is increasing interest in the internal circulation of both natural and constructed wetlands to better understand and model their ecology, nutrient and pollutant removal, and water-storage abilities (Hopkinson et al. 1988; Mitsch and Gosselink 2000). Models for the marsh regions within wetland systems often assume uniform vegetation, which is represented by uniform hydraulic roughness and dispersion constants (Jadhav and Buchberger 1995; Bolster and Saiers 2002; Persson 2005). When no dispersion is present, this assumption results in plug flow, in which all water entering the marsh spreads out across the width and remains in the marsh for exactly the hydraulic residence time $\tau = V/Q$, where V is the marsh volume and Q the volumetric flow rate through it. However, velocity heterogeneity is nearly always present in wetlands and results in some influent water remaining in the wetland for a time much shorter

than the mean residence time. For example, in a 0.81-km² wetland in Florida, 32% of the flow exits the wetland in only 0.3τ (Keller and Bays 2002). This phenomenon, known as short-circuiting, results in zones of different local residence time that can generate distinct biogeochemical zones (Harvey et al. 2005), which in turn may influence the diversity of available habitats. In addition, biogeochemical processes and uptake rates depend on local water velocities (Eriksson 2001). In treatment wetlands, such heterogeneity nearly always results in reduced contaminant removal (Wörman and Kronnäs 2005). Understanding and accounting for short-circuiting is therefore vital for constructing accurate and useful models of wetland systems (Bolster and Saiers 2002).

Fast flow paths, which carry short-circuiting water, often result when a portion of the wetland lies below the average marsh elevation. An extreme example is a tidal creek system, in which flow is dominated by transport within incised creek channel networks that are clearly visible in aerial photographs (Arega and Sanders 2004). In many natural wetlands, macrophytes fringe a central, deeper open channel, with a large fraction of the flow carried by that channel (Cooper 1994). For example, Stern et al. (2001) observed that a central channel carried more than 50% of the flow in a natural wetland in Westchester, New York. Similarly, within the ridge and slough landscape in the Everglades National Park in Florida, water velocities are slower within elevated tree islands than in the surrounding deeper marshes (Bazante et al. 2006). Constructed wetlands may also have deep channels that create preferential flow paths. For example, within the Everglades Nutrient Removal Project in Florida, abandoned agricultural ditches and borrow canals oriented parallel to flow

¹To whom correspondence should be addressed. Present address: St. Anthony Falls Laboratory, University of Minnesota, 2 Third Ave. SE, Minneapolis, MN 55414 (annel@umn.edu).

²Present address: Department of Civil and Environmental Engineering, University of Washington, More Hall, Box 352700, Seattle, Washington 98195-2700.

Acknowledgments

We are grateful to the staff at the Southeastern Natural Sciences Academy, especially Gene Eidson and Oscar Flite, and at Operations Management International, Inc., for enabling site visits to the Augusta municipal treatment wetlands in August 2005 and July 2006. We also thank Jim Bays from CH2M HILL for his support and two anonymous reviewers for their comments.

This material is based upon work supported by the Switzer Foundation, the Martin Family Foundation, a National Science Foundation Graduate Research Fellowship, and the National Science Foundation under grant EAR 0309188.

create dramatic short-circuiting (Guardo and Tomasello 1995; Dierberg et al. 2005).

However, not all fast flow paths are marked by a different elevation, and those that are not are more difficult to identify. For example, soil oxygen availability, microtopography, and vegetation clonal reproduction can interact to create patches of different types of vegetation (Marani et al. 2006), and changes in vegetation type and density can lead to differential travel times (Stern et al. 2001). Large interspersed patches of submerged aquatic vegetation and emergent cattail stands likely contributed to the observed velocity heterogeneity in the Everglades Nutrient Removal Project (Nungesser and Chimney 2006). Over time, vegetation heterogeneity can develop into discernable flow paths. For example, Bays and Knight (2002) observed small flow paths in a portion of a 10-yr-old 0.06-km² constructed wetland in Fort Deposit, Alabama. Kjellin et al. (2007) report that sparse vegetation contributed to short-circuiting in a treatment wetland in Ekeby, Sweden. It is likely that some amount of short-circuiting is always present in vegetated systems (Kadlec and Knight 1996).

Further complicating flow patterns, most natural wetlands, and many constructed wetlands as well, contain pockets of deeper open water interspersed with the vegetated marsh areas. These deep zones provide many important functions, including an increase in habitat diversity, a quiescent area that promotes sedimentation, and refugia for fish and other wildlife in dry weather (Sartoris et al. 2000; Bays and Knight 2002). Successful models of flow through wetlands must account for interactions between deep and shallow areas with different vegetation densities (Feng and Molz 1997). However, flow interactions and exchange between deep zones and marsh areas are still not well understood. For example, flow patterns may be complicated by convective currents driven by temperature differences between shallow, vegetated regions and deep, unvegetated regions (James and Barko 1991).

This paper uses detailed field measurements to characterize the velocity heterogeneity within a shallow emergent marsh region as well as the interaction of fast flow paths with deep open-water zones. To date, the contribution of short-circuiting to overall flow through a wetland has only been inferred from wetland-scale tracer studies. Here, flow measurements and tracer studies are performed within a 1.5-km² constructed treatment wetland in Augusta, Georgia to directly quantify the size, distribution, and velocity of the fast flow paths through marsh areas. In addition, the water traveling within fast flow paths was tracked as it entered an open-water region. Secondary goals of this study were to quantify both the amount of lateral mixing present within a deep open-water zone receiving short-circuiting flow and the temperature differences between shallow vegetated and deep open-water zones.

Site description

Field observations were performed during July 2006 within the 1.5-km² constructed treatment wetlands associ-

ated with the J. B. Messerly Wastewater Treatment Plant (WWTP) in Augusta, Georgia (33.38°N, 81.95°W, Fig. 1). The wetlands were built between 1997 and 2002 to provide additional nitrogen removal from treatment plant effluent before it is discharged to the Savannah River. Observations were performed within 3 of the 12 wetland cells. During the construction of each of these cells, grading was used to remove natural microtopography, and the remaining bottom topography was configured into an alternating pattern of shallow marshes and deep zones (Fig. 2). Construction of cell 12 was completed in 2000; construction of cells 6 and 7 was finished in 2002. In all three of these cells, plugs of *Zizaniopsis miliacea*, *Typha* sp., and *Scirpus* sp. were planted uniformly on 1-m centers in marsh regions (Eidson and Flite 2005). Aerial observations confirmed that the vegetation had successfully colonized the entire marsh surface and that the dominant remaining species was giant cutgrass, *Z. miliacea*.

During July 2006, the shallow marsh regions of the cells had a water depth of $h_m = 48 \pm 2$ cm, although bottom wrack occluded much of the flow area and limited active water flow to within 15 to 30 cm of the water surface. The deep zones had a water depth of $h_{dz} = 130 \pm 7$ cm (average of 18 measurements). Each cell has a total length $L \approx 550$ m and a total width B between 207 ± 3 m and 254 ± 3 m (Fig. 2). Within each cell, there are three transverse deep zones (including the final deep collection area), each with a length $L_{dz} = 48 \pm 9$ m. Each deep zone has an entrance slope of 12–17° (range of 18 measurements). The volume of water in each wetland cell is $V \approx 68,000$ m³. The primary vegetation in the marsh region, *Z. miliacea*, typically has a stem diameter $d \approx 3$ cm (Fox and Haller 2000) and would be expected to have a stem density of 100 m⁻² (Campagna and Marques 2001), so its solid volume fraction $\phi \approx 0.1$.

Steady flow conditions were present within the Messerly wetlands during July 2006. Flow exiting the WWTP entered a settling pond and then a distribution canal, from which weirs controlled the flow rate into each of the 12 individual cells. According to WWTP records, the flow rate entering the wetland system was $1,170 \pm 20$ L s⁻¹ and was approximately constant over the course of the study (Fig. 3A). Neither entrance nor exit weirs in the individual cells were adjusted over the duration of the study. Data from a previous study within this wetland imply that under steady flow conditions the flow rate entering each cell, Q , is 1/12 of the total wetland discharge with an uncertainty of $\pm 30\%$ (Flite et al. 2006). The same study suggests that infiltration and evapotranspiration within this wetland are negligible compared with the average discharge Q , so the flow rate entering and leaving each of the wetland cells depends primarily on the plant flow rate (Flite et al. 2006). The United States Geological Survey (USGS) gage station (Sta. 02196999) at the Savannah River Lock and Dam, located 1 km away, recorded a total of only 3 cm of rainfall between 01 July and 31 July 2006 (Fig. 3B). The flow rate entering and exiting each cell was therefore $Q = 100 \pm 30$ L s⁻¹, for a hydraulic loading rate $= Q/BL \approx 4$ cm d⁻¹. The nominal residence time $\tau = V/Q \approx 8$ d within each cell. The mean, or plug-flow, velocity in the cell is $U_{PF} =$

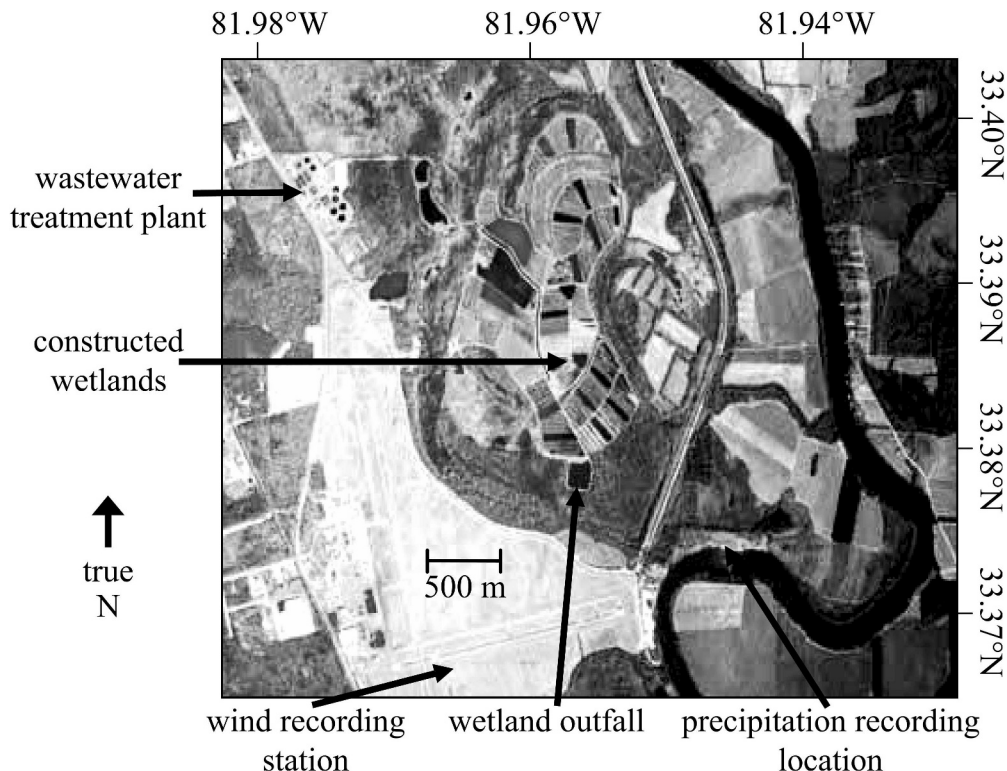


Fig. 1. Relative locations of the Messerly constructed treatment wetland, the wastewater treatment plant that discharges into it, and its outfall to a stream that discharges into the Savannah River. The locations of the USGS precipitation and NOAA wind and air temperature measurement stations are also shown. Color-infrared image taken 04 March 2006 by the United States Department of Agriculture.

$Q/(Bh[1 - \phi]) = 0.1 \text{ cm s}^{-1}$. If no short-circuiting or dispersion is present, the time for water to travel a length ΔL will be:

$$t_{\text{PF}} = \Delta L / U_{\text{PF}} = \frac{\Delta L B h (1 - \phi)}{Q} \quad (1)$$

Wind speed and direction were recorded at the National Oceanic and Atmospheric Administration (NOAA) weather station at the Augusta airport (KAGS), less than 2 km away. The wind speed at 10 m above the surface, U_{10} , had a strong diurnal pattern of intensity (Fig. 4A) and also varied direction over the course of the study (Fig. 4B). Air temperature was recorded at the same station (Fig. 3C).

Methods

Tracer studies were used to determine the degree of short-circuiting within one vegetated marsh section in each of three different cells. The sampling areas within cells 6 and 7 were the vegetation just upstream of the first deep zone; the sampling area in cell 12 was the vegetation just upstream of the second deep zone. Dye was released across the entire cell twice at each site: cell 6 beginning at 10:52 h on 12 July and 09:27 h on 21 July, cell 7 at 09:47 h on 19 July and 08:38 h on 24 July, and cell 12 at 09:23 h on 18 July and 09:54 h on 26 July. Each study consisted of the

release of a known volume between 100 and 1,000 mL of intracid rhodamine WT (Crompton and Knowles 20% liquid solution, density = 1.1 g L^{-1}) in a line across the cell upstream of a region of dense vegetation of length L_{dye} between 34 ± 5 and 38 ± 5 m. Dye was injected using a field pump, which was towed across the cell at $0.3\text{--}0.4 \text{ m s}^{-1}$, pumping at a constant rate of 200 mL min^{-1} . To rapidly dilute the dye and reduce density effects, the dye was immediately stirred into an approximately 1-m-wide swath of surrounding water. Over a week or more, rhodamine WT is not conservative and will adsorb to sediments and plant matter, which will result in an underestimation of travel times during a full-scale wetland study (Cooper 1994; Lin et al. 2003; Keefe et al. 2004). However, it has been used successfully in short-term studies of less than 6 d (Stern et al. 2001; Lin et al. 2003). Each of the studies reported here was less than 96 h long.

The appearance of the dye downstream of the vegetation was detected by towing an in situ fluorometer (Seapoint Sensors) connected to a conductivity-temperature-depth probe (Ocean Sensors) within the deep zone along the downstream edge of the vegetation. The fluorometer sampled at 8 Hz and its voltage output was calibrated using known concentrations of the rhodamine stock solution diluted in freshwater. Sampling continued up to 96 h after each release. The depth of the fluorometer was varied on different lateral traverses, which each took

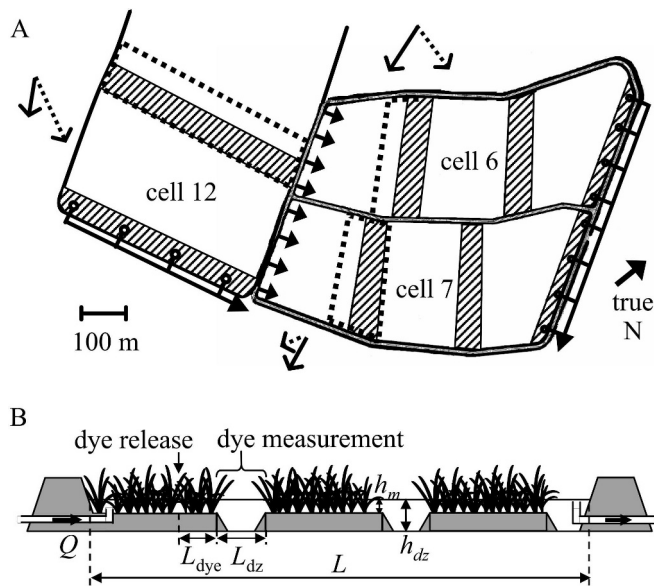


Fig. 2. (A) Plan view of the three studied cells. Deep zones are marked by hatching. Dotted lines surround the regions where dye studies were performed. The solid arrows with line heads indicate the average speed and direction of the wind over the full duration of the deep-zone dye release experiments shown in Fig. 9; the dotted arrows with line heads indicate the average speed and direction of the wind during the first 6 h after those releases. Solid arrows with full heads and circles indicate the location of flow inlet and outlet structures, respectively. (B) Schematic side view of a longitudinal cross-section through one of the cells, highlighting the bathymetry of the deep zones and the location of dye injection and measurement. Not to scale. Flow is from left to right.

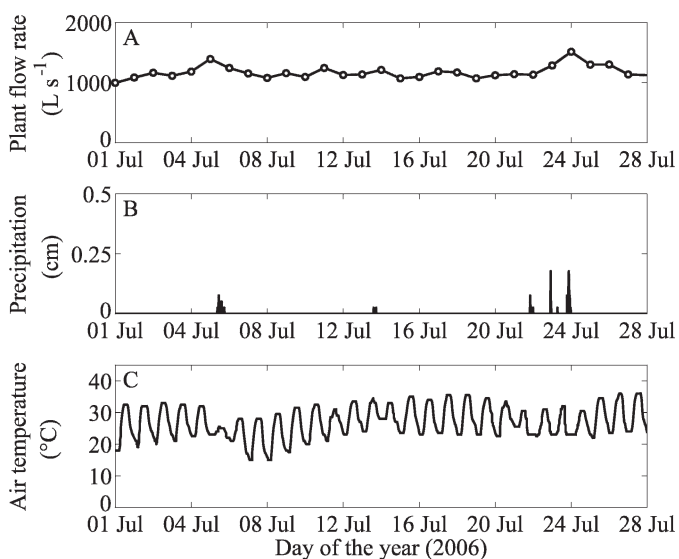


Fig. 3. (A) Plant flow rate discharging into the distribution pond upstream of all 12 wetland cells. (B) Precipitation recorded in 15-min intervals at nearby USGS gaging station. (C) Air temperature recorded at nearby NOAA station.

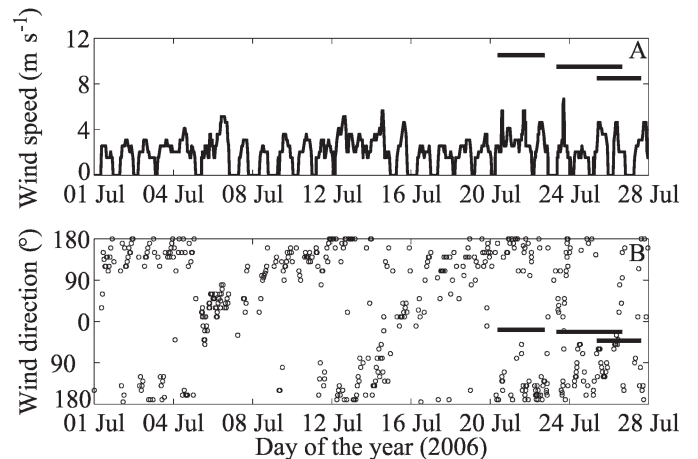


Fig. 4. (A) Wind speed (U_{10}) recorded at nearby NOAA station. Horizontal bars indicate the duration of the deep-zone tracer experiments shown in Fig. 9. (B) Direction from which wind is blowing in degrees from true north recorded at nearby NOAA station. Horizontal bars indicate the average wind direction over the duration of the tracer experiments.

approximately 15 min. To record boat position accurately, stakes were placed at 8- to 60-m increments across the width of the deep zones, and records were kept of the time the boat passed each stake. Linear interpolation was then used to determine boat position between stakes. A handheld global positioning system unit (eTrex Venture, Garmin, ± 5 m accuracy) was used to spot-check the stake and boat positions.

Fast flow paths were assumed to exist upstream of the regions at which dye was first observed within the deep zone. In particular, a fast flow path was defined as contributing more dye than the lateral average during the first $t_{PF}/2$ after release. For each tracer study, the concentration recorded before $t_{PF}/2$ after release was interpolated using a triangle-based cubic fitting algorithm to a 1-min by 0.25-m grid and integrated over time to find the average concentration, $C_{avg}(y)$, during this time interval. In addition, at each lateral position where $C_{avg}(y)$ was higher than its average value across the cell width, the arrival time of the peak concentration, t_{dye} , was used to estimate the average transit time of tracer through the fast flow paths, $u_{dye} = L_{dye}/t_{dye}$. To estimate the uncertainty in these calculations, several point releases were performed with the fluorometer fixed directly at the outlet of an identified flow path. These continuous point records were then resampled at 20-min intervals, which was the average interval between successive traverses, and used to calculate values of C_{avg} and t_{dye} . The reported uncertainties associated with the C_{avg} and t_{dye} values are the sum in quadrature of the differences between the values calculated from the continuous point measurements, the resampled point measurements, and the traverse measurements.

In the areas identified as fast flow paths, detailed observations of flow speed were then undertaken using small-scale releases of a nonfluorescent tracer (food coloring), surface floaters, and a two-dimensional side-ways-looking acoustic Doppler velocimetry (ADV) probe

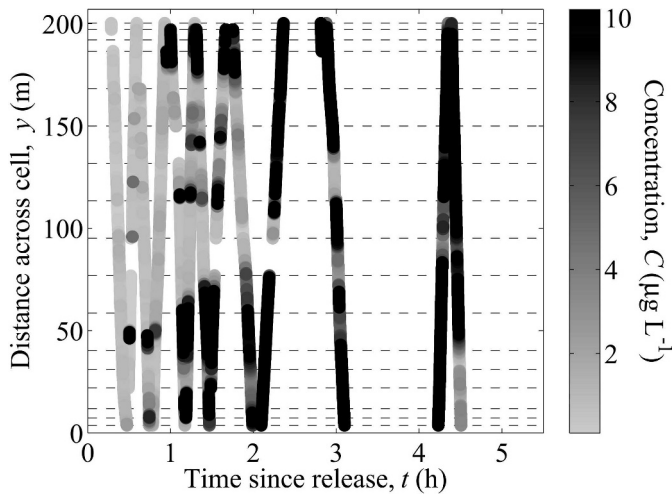


Fig. 5. Sample breakthrough curve of dye exiting a 38-m-long swath of continuously vegetated marsh in cell 7. Each point measurement is shaded to represent measured rhodamine WT concentration. Horizontal dashed lines mark the position of reference stakes on the bank. The release was on 19 July and the expected time to exit is $t_{PF} = 11 \pm 4$ h.

(Flowtracker, SonTek/YSI). The Flowtracker acquired 1-min-long point measurements of the water velocity exiting the densely vegetated regions. Preliminary analysis confirmed that 1 min was long enough for the measurement to reach a stable mean value; only mean flow was resolved or will be discussed. Factory specifications state that the Flowtracker is capable of measuring between 0.1 cm s^{-1} and 500 cm s^{-1} with an accuracy of 1%, though we were unable to attain satisfactory precision for $u < 0.5 \text{ cm s}^{-1}$ (cf. Bazante et al. 2006). The ADV probe was fixed to a staff gage resting on the marsh bed. Before each measurement, wrack and vegetation were removed from the 10-cm-wide area between the probe arms and the sampling volume. We focused the ADV measurements around the fast-flowing regions identified by the tracer study.

A ruler was used to measure the depth h_m and width b_f of each fast-flow region. The lateral flow-path boundaries were assumed to exist at the nearest cutgrass clump on either side of the main flow path, which, as shown by detailed flow measurements in several fast flow paths, coincided with the location where the flow velocity decreased below the detection limit. B_f represents the total width of fast flow paths within a cell, such that $B_f = \Sigma b_f$.

Velocity records were used to estimate flow rates through the fast flow paths as follows. The velocity distribution in each fast flow path was normalized by the peak velocity, the flow-path width, and the full flow-path depth. The normalized data from all fast flow paths were then pooled to create a composite velocity distribution. The composite profile was integrated over depth and width to define the scale factor β between the average velocity u_f and the peak velocity u_{peak} within a fast flow path, such that $u_f = \beta u_{peak}$. The error associated with the scale factor was estimated as the standard deviation of subgroup scale factors estimated for 50 random subsamples of 25

measurements each. The flow rate for each fast flow path was then calculated as $q_f = u_f h_m b_f = \beta u_{peak} h_m b_f$. The total flow, Q_f , through the n_f fast flow paths within a given cell was estimated by summing the individual flow rate measurements from all fast flow paths within the cell: $Q_f = \Sigma q_f$. The fraction of flow carried by fast flow paths is given by Q_f/Q . The average flow velocity along the fast flow paths is given by $U_f = Q_f/B_f h_m$. From continuity, the depth-averaged velocity along the slow-flow zones is given by:

$$U_s = \frac{Q - Q_f}{h_m(B - B_f)(1 - \phi)} \quad (2)$$

To characterize transport within the open-water deep zones, the fluorometer was also used to make periodic lateral transects at eight staked longitudinal positions within the deep zone downstream of the studied marsh region. Dye concentration was measured for up to 96 h after one dye release within each cell: 09:27 h on 21 July in cell 6, 08:38 h on 24 July in cell 7, and 09:54 h on 26 July in cell 12. Before analysis, synoptic results were averaged over depth and interpolated to a $1\text{-m} \times 1\text{-m}$ grid. The data resolution was not high enough to identify the 1% or even 10% contour, so the longitudinal extent of the evolving tracer clouds was defined as the location where the concentration equaled 30% of the maximum concentration observed at that time. The speed of the tracer cloud was calculated as the rate of change in the longitudinal position of the tracer front.

Temperature loggers (HOBO temperature logger, Onset Computer Co.) were deployed during each dye release. At least three loggers were placed on a thermistor chain in the middle of the deeper open-water area, two loggers were placed at mid-depth within dense vegetation 5 m upstream of the deep zone, and one logger was placed within an identified fast flow path 5 m upstream of the deep zone. When multiple loggers were deployed simultaneously in similar sites, temperature data were averaged and the difference in measurements used to estimate uncertainty. To create a composite daily temperature cycle for each position, the nightly minimum temperature was subtracted and results were conditionally averaged over the 24 d of deployment.

Results and discussion

Flow and transport through vegetated regions—In each of the three cells examined, tracer studies revealed the presence of multiple fast flow paths distributed across the width of the cell. As an example, Fig. 5 shows concentration transects measured at the downstream end of a swath of dense cutgrass of length $L_{dye} = 38 \pm 5$ m. Distance across the cell is plotted on the y -axis; the x -axis is time. Gray scale denotes measured concentration. Because of boat turning, we were unable to sample within 4 m of each side bank. If uniform flow existed within the vegetation, the peak concentration would be observed at $t_{PF} = 11 \pm 4$ h (Eq. 1), where the major source of uncertainty is from the cell flow rate Q . Figure 5 shows tracer exiting the

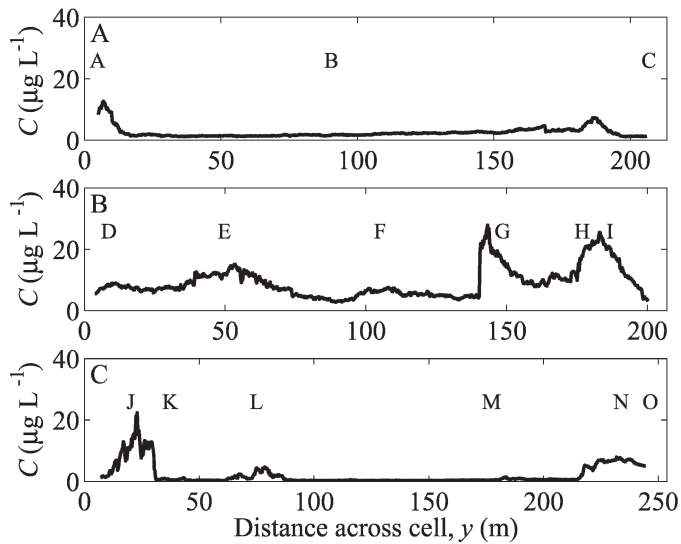


Fig. 6. Concentration measured exiting a 34- to 38-m-long swath of continuously vegetated marsh in three wetland cells: (A) cell 6 on 12 July, (B) cell 7 on 19 July, and (C) cell 12 on 18 July. The plotted concentration is the average recorded at each lateral position before $t_{PF}/2$. Each concentration peak is marked with a letter and described in more detail in Table 1.

vegetation before $t_{PF}/2$; this value was used as a cutoff, because marked fluid that emerged in less than this time was clearly traveling much faster than the mean flow velocity through the cell. Tracer was detected at several distinct lateral positions as early as $t = 29$ min after tracer release, indicating the presence of several short-circuiting pathways.

Figure 6 shows the time-averaged concentration profile recorded up to $t_{PF}/2$ after release within all three studied cells. Results with concentration peaks at similar locations were obtained for a repeat dye release within each of these cells (not shown). Between the peaks, dye concentrations were typically below the detection limit of the fluorometer. The dye studies in Fig. 6 were used as a guide in identifying fast flow paths. The lateral position of each fast flow path, which was confirmed by visual inspection, is indicated by a letter in Fig. 6. In instances where we found two fast flow paths separated by less than 2 m, we considered the sum of the two to be one flow path. Within each of the three cells, between three and six distinct flow paths transported more dye than the average. Because of time constraints, fast flow paths F, G, and L were only characterized by the tracer study; the average of the other fast flow paths was used when calculating total values for each cell. Flow path C was located too close to the bank to identify using the boat-mounted fluorometer but was identified on foot when performing velocity measurements.

More detailed tracer studies were conducted at flow path A. Two types of measurements were taken. First, the fluorometer was fixed in one horizontal location, and the concentration at different depths was recorded (Fig. 7A). The peak concentration was recorded at $z = 11$ cm below the surface, and concentrations above background were observed down to 6 cm above the bed ($z = 46$ cm).

Figure 7B compares observations between a fluorometer fixed at the flow path exit and a fluorometer making lateral traverses while mounted on a boat. The vertical axis shows the recorded concentration, normalized by the concentration at the location of the line source. The horizontal axis shows the time since the release occurred a distance $L_{dye} = 37 \pm 5$ m upstream. Note that the peak arrival times from the fixed and traverse measurements are similar, suggesting that the transit time calculated from the lateral traverses is comparable with what would have been observed using multiple stationary recording fluorometers. In addition, the five curves represent five different releases on three different days, yet they produced concentration responses with similar peak arrival times, confirming the repeatability of these measurements and the steadiness of the flow pattern. Four of the five also exhibited similar peak concentrations; it is likely that the peak concentration on the fifth transect was observed when the fluorometer was located at a slightly different position relative to the center of the plume. Finally, even though $t_{PF} = 11 \pm 4$ h, the center of mass of recovered dye occurred only 34 ± 2 min (mean of five measurements) after release, verifying that this is a region of elevated velocity, with flow 13 times faster than the mean flow $U_{PF} \approx 0.1$ cm s⁻¹, and also that $t_{PF}/2$ is sufficiently long to identify the center of mass.

ADV measurements revealed that these fast flow paths had a maximum velocity up to $u_{peak} = 7.8$ cm s⁻¹ (Table 1). The sample velocity transect shown in Fig. 8A, taken at the depth of peak velocity, illustrates that the velocity measured for water exiting the fast flow paths was much higher than that measured in the slow-flow zones on either side. Because the ADV instrument was unreliable below 0.5 cm s⁻¹, it can only be concluded that the velocity exiting the vegetation was less than 0.5 cm s⁻¹; from Eq. 2, the depth-averaged velocity U_s should be less than U_{PF} .

The parameters describing each fast flow path are presented in Table 1. The average fast flow path width was $b_f = 2.5 \pm 0.5$ m. The total width of fast flow paths was $B_f = \sum b_f = 3 \pm 1$ m, 11 ± 1 m, and 21 ± 1 m in cells 6, 7, and 12, respectively (Table 2). The widths of these cells were, respectively, $B = 213 \pm 3$ m, 207 ± 3 m, and 254 ± 3 m, so the fraction of area occupied by fast flow paths was, respectively, $B_f/B = 0.016 \pm 0.004$, 0.05 ± 0.01 , and 0.08 ± 0.01 in cells 6, 7, and 12. Note that these numbers reflect what was observed. It is possible that other flow paths were present but not identified. These numbers therefore provide a lower bound on the fraction of short-circuiting flow within these wetland cells.

Detailed measurements of the velocity profile were carried out within several fast flow paths. In all velocity distributions, the velocity peak was near the middle of the flow path and within the upper third of the water column. We had at least one measurement within that zone within each fast flow path. The vertical velocity profile was not logarithmic, and in fact a substantial region near the bed had no flow because of accumulated dead vegetation (e.g., the lower 13 cm of the water column in Fig. 8A). The horizontal velocity profile also deviated from that within a banked channel because the edges of the fast flow paths were porous, consisting of clumps of vegetation that

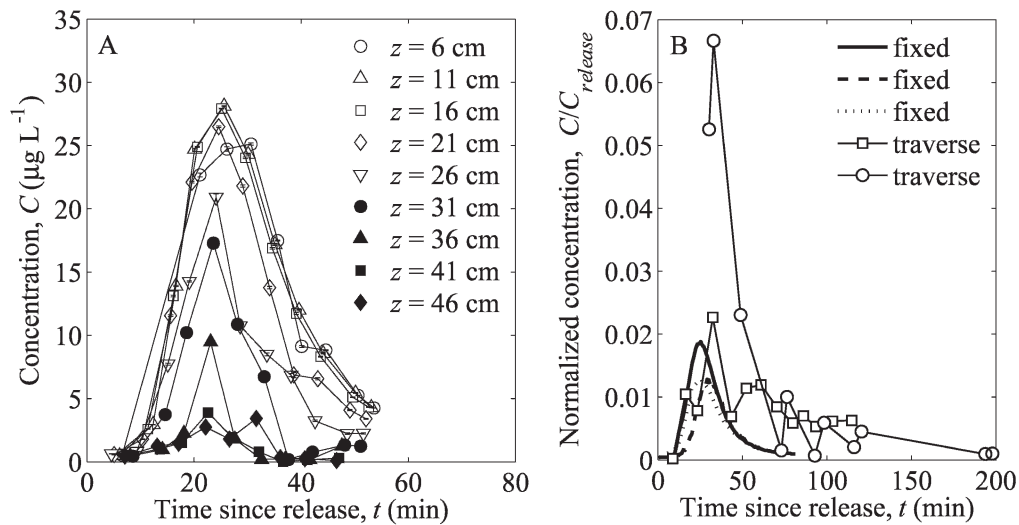


Fig. 7. Records of concentration exiting a fast flow path (flow path A in Table 1). (A) Detailed measurements of dye concentration at different depths a few meters downstream of the flow path mouth, where the local water depth was 52 cm and z indicates depth below surface. (B) Records of concentration exiting from flow path A, normalized by the mixed concentration just after release. In the “fixed” observations, the recording fluorometer was placed at a stationary location in the middle of flow path A and dye was injected at a single location directly upstream. In the “traverse” observations, the fluorometer was located on a boat that was traversing the wetland, and dye was injected across the width of the cell. The expected plug-flow time of transit is $t_{\text{PF}} = 11 \pm 4$ h.

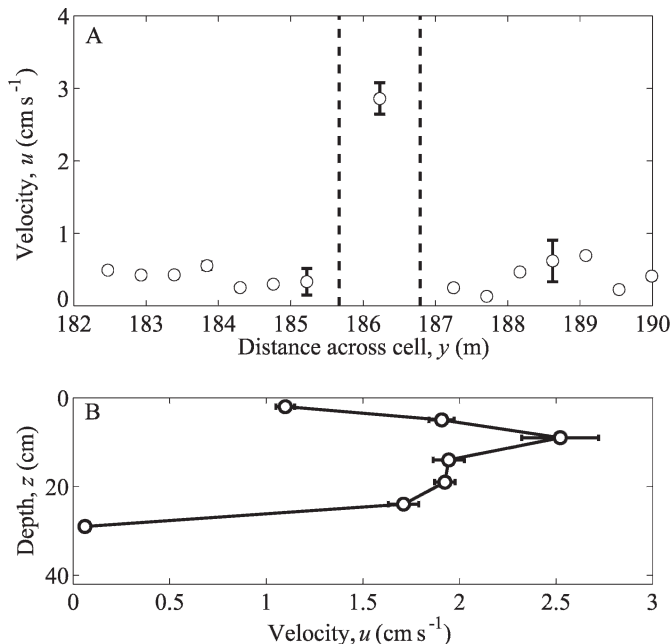


Fig. 8. Sample point measurements of water velocities exiting dense vegetation. (A) Transect across the mouth of a fast flow path (flow path B in Table 1). Vertical dashed lines indicate the edges of the flow path, which had a width $b_f = 1.1 \pm 0.1$ m. From continuity, the expected slow-flow zone velocity was $U_s \approx 0.1$ cm s^{-1} . Vertical bars indicate the standard error of the mean velocity at each lateral position. (B) Vertical transect at the midline of a fast flow path (flow path I). The total marsh water depth was $h_m = 42 \pm 1$ cm. Horizontal bars indicate the standard error of the mean velocity at each vertical position.

contributed roughness and allowed limited momentum exchange. A composite velocity profile constructed from 96 velocity measurements within 15 fast flow paths indicated that the average velocity u_f over the path cross-section was $32\% \pm 7\%$ of the peak measured velocity: $u_f = (0.32 \pm 0.07)u_{\text{peak}}$. Among the several fast flow paths, the average velocity u_f varied between 0.3 and 2.7 cm s^{-1} . Note that the average velocities observed at the fast flow path exit u_f are the same order of magnitude as and roughly proportional to the velocities inferred from the mean travel time of tracer through the vegetation (u_{dye} in Table 1), showing that the two methods are consistent and suggesting that the fast flow paths are coherent through the vegetated marsh region. Similarly, previous work found that a fast-moving stream has limited exchange with surrounding dense vegetation (Su and Li 2002).

The average velocity u_f for each identified fast flow path and its measured dimensions were combined to produce the flow rate q_f within that flow path (Table 1). For cells 6, 7, and 12, the total volume of fast flow $Q_f = \sum q_f$ was 18 ± 2 L s^{-1} , 45 ± 5 L s^{-1} , and 64 ± 13 L s^{-1} , respectively (Table 2). When compared with the average flow through the cells ($Q = 100 \pm 30$ L s^{-1}), these data indicate that the fraction of flow traveling within fast flow paths was $Q_f/Q = 0.2$ – 0.7 . The ratios between the fast-flow velocity and the mean velocity are $U_f/U_{\text{PF}} = 8$ – 12 and the ratios between the fast and slow velocities in each cell are $U_f/U_s = 14$ – 20 . These results suggest that at least 20% of the flow has a residence time that is less than one-eighth of the nominal residence time.

Similar ratios can be estimated for other wetlands. For example, in a tracer study at a 0.77- km^2 wetland in central Florida, the peak tracer concentration at the outlet was observed after 0.4 d, whereas the nominal residence time was 19 d (Keller and Bays 2002), suggesting that the peak

Table 1. Dimensions and velocity measurements for each fast flow path identified in Fig. 6. The columns provide the following information: the letter designation of each flow path (see Fig. 6); the cell where it is located; the lateral position of the flow path, y ; the width of the flow path, b_f ; the average water depth within the flow path, h_m ; the travel speed of the center of mass of dye emerging from the flow path, u_{dye} ; the peak measured velocity within the flow path, u_{peak} ; the area-average velocity within the flow path, u_f ; and the average flow rate within the flow path, q_f . Dashes indicate locations where direct measurements were not taken.

Flow path	Cell	y (m)	b_f (m)	h_m (m)	u_{dye} (cm s ⁻¹)	u_{peak} (cm s ⁻¹)	u_f (cm s ⁻¹)	q_f (L s ⁻¹)
A	6	5±3	0.7±0.1	0.28±0.01	1.6±0.5	7.8±0.1	2.7±0.2	5±1
B	6	186±3	1.1±0.1	0.44±0.01	1.9±0.6	3.2±0.2	1.1±0.2	6±1
C	6	207±3	1.6±0.1	0.45±0.01	-	2.9±0.3	1.0±0.2	7±2
D	7	9±3	2.4±0.1	0.45±0.01	0.7±0.2	2.5±0.2	0.9±0.2	10±2
E	7	49±3	1.4±0.1	0.43±0.01	0.9±0.2	4.4±0.5	1.5±0.2	9±2
F	7	105±3	2.4±0.1	0.48±0.01	1.0±0.3	-	-	-
G	7	145±3	2.4±0.1	0.48±0.01	0.5±0.1	-	-	-
H	7	180±3	1.3±0.1	0.44±0.01	0.5±0.1	0.8±0	0.3±0.2	2±1
I	7	186±3	0.9±0.1	0.42±0.01	0.5±0.1	2.3±0.7	0.8±0.4	3±1
J	12	20±3	3.8±0.1	0.57±0.01	0.5±0.1	0.8±0.1	0.3±0.2	6±5
K	12	37±3	8.2±0.1	0.53±0.01	0.4±0.1	1.0±0.1	0.3±0.2	15±10
L	12	75±3	2.4±0.1	0.48±0.01	0.3±0.1	-	-	-
M	12	221±3	2.7±0.1	0.53±0.01	0.6±0.2	1.4±0.1	0.5±0.2	7±3
N	12	234±3	1.2±0.1	0.60±0.01	0.6±0.2	3.0±0.1	1.0±0.2	7±2
O	12	246±3	3.2±0.1	0.60±0.01	0.7±0.2	2.8±0.1	1.0±0.2	18±4

concentration traveled through a short-circuiting flow path for which $U_f/U_{PF} \approx (19 \text{ d})/(0.4 \text{ d}) = 48$. Tracer test data from four cells in the Orlando Easterly Wetland suggest that $U_f/U_s = 2\text{--}22$ and the ratio of fast flow path flow rate to total flow rate $Q_f/Q \approx 0.5$ (Martinez and Wise 2003).

The (perhaps unavoidable) development of fast flow paths should be considered when planning any large tracer study. Traditionally, tracer studies are planned on the basis of the nominal residence time; for example, Frossard et al. (1996) recommend a first sample at 0.1τ . However, the presence of short-circuiting means that a large fraction of dye will emerge well before τ , and using τ in planning calculations can result in undersampling the peak (Keller and Bays 2002). Note also that, because a wetland is not laterally homogeneous, it is not valid to assume that

multiple outlets within a wetland will have the same residence time distribution (RTD) (Keller and Bays 2002), because outlets directly downstream of a fast flow path can have a very different RTD from outlets in regions without fast flow paths.

Transport through unvegetated deep zones—After the water flowed out of the marsh region, it entered a transverse deep zone (Fig. 2). Figure 9A shows the spatial distribution of dye within the deep zone in cell 6 at various times after a release within the marsh upstream. Within each subplot, the axes represent the x - y coordinates, and the gray scale indicates the average concentration over depth. The advective time of transit, t_{PF} , was 11 ± 4 h through the marsh and 37 ± 16 h to the downstream edge

Table 2. Average short-circuiting parameter values for each studied cell. Mass values are shown for the second release in each cell (e.g., results in Fig. 9).

Parameter	Units	Cell 6	Cell 7	Cell 12
Cell width, B	m	213±3	207±3	254±3
Cell flow rate, Q	L s ⁻¹	100±30	100±30	100±30
Dye travel length, L_{dye}	m	37±5	38±5	34±5
Deep-zone length, L_{DZ}	m	49±2	49±8	44±5
Plug-flow velocity, U_{PF}	cm s ⁻¹	0.10±0.03	0.10±0.03	0.08±0.02
Plug-flow transit time, t_{PF}	h	11±4	11±4	12±4
Number of fast flow paths, n_f	—	3	6	6
Total width of fast flow paths, B_f	m	3±1	11±1	21±1
Total flow rate of fast flow paths, Q_f	L s ⁻¹	18±2	45±5	64±13
Average fast flow path velocity, U_f	cm s ⁻¹	1.1±0.1	0.9±0.1	0.6±0.1
Average slow-flow zone velocity, U_s	cm s ⁻¹	0.09±0.03	0.06±0.03	0.03±0.02
Mass released, $M_{release}$	g	910±10	870±10	1,110±10
Mass recovered before $t_{PF}/2$, M_f	g	180±80	260±100	470±70
B_f/B	—	0.016±0.004	0.05±0.01	0.08±0.01
Q_f/Q	—	0.2±0.2	0.5±0.2	0.7±0.2
U_f/U_s	—	14±3	15±3	20±3
U_f/U_{PF}	—	12±3	9±3	8±3
$M_f/M_{release}$	—	0.20±0.09	0.30±0.12	0.42±0.06

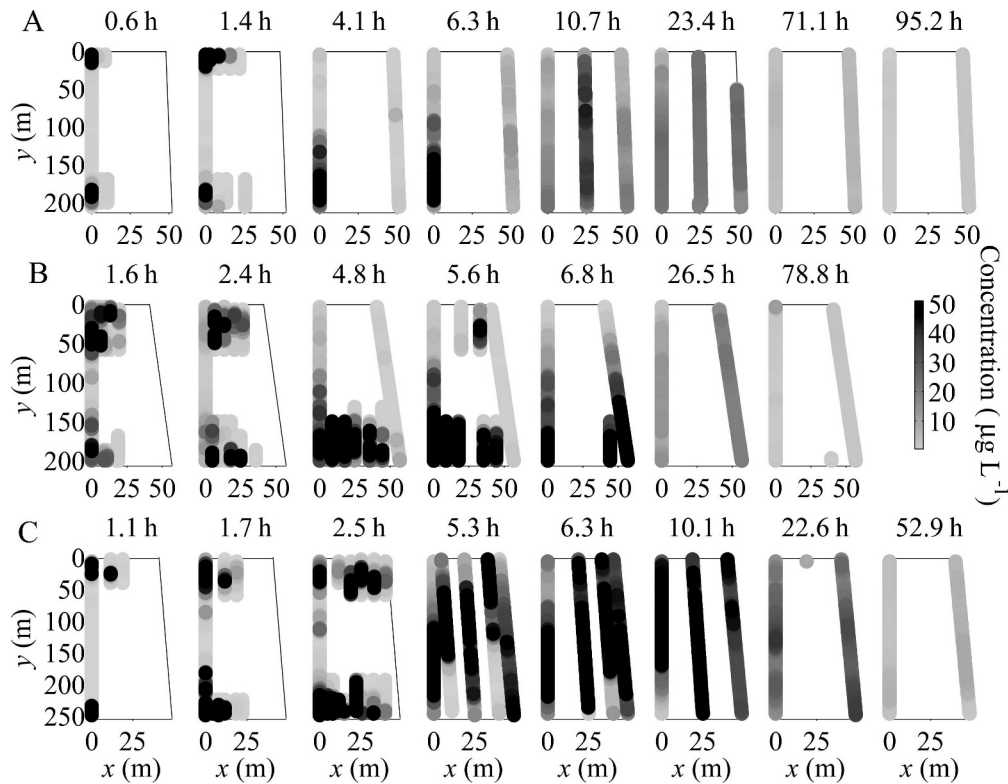


Fig. 9. Tracer concentrations at various times after release within an open-water deep zone in (A) cell 6, (B) cell 7, and (C) cell 12. The panel shape indicates the shape of the deep zone. When available, multiple measurements obtained within a 30-min time frame at the same horizontal position are averaged together.

of the deep zone. Figure 9B,C shows the results for similar releases in cells 7 and 12, for which the plug-flow times of transit from the release location to the downstream edge of the deep zone were 35 ± 15 h and 40 ± 17 h, respectively.

The advance of the tracer front, here defined as the location where the concentration equaled 30% of the maximum concentration observed at that time, can be used to estimate the speed of the advection of fast-flow water within the deep zone. Tracer reached the downstream edge of the deep zone approximately 25 to 30 h after release, which is slightly less than the 35 to 40 h expected for advective transport. Because tracer reached the downstream edge of the deep zone before it mixed laterally, it was possible to distinguish the evolving plumes from flow paths in different halves of the deep zone, and the position of the dye front was calculated for each lateral half of the deep zone separately. Similarly, in a numerical simulation of a tracer released at the entrance to a wide but short stormwater pond, Walker (1998) found that dye exited the system well before it mixed laterally. Figure 10 shows the speed of the dye front for the three releases shown in Fig. 9. The speed of the tracer front decayed to background within 5–10 m of the beginning of the deep zone, after which the tracer traveled across the deep zone at a speed at the same order of magnitude as the expected plug-flow velocity u_{PF} . The thick layer of periphyton near the bed of the deep zone may have contributed to this rapid decay of fast-flow momentum.

Although the tracer front (30% contour) progressed slowly across the deep zone, tracer concentration above

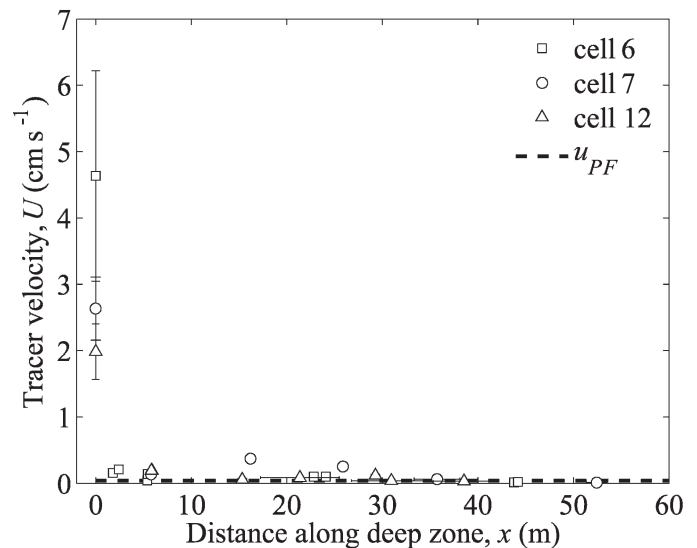


Fig. 10. Estimated velocity of the front of the tracer cloud as a function of distance into the deep zone for the tracer releases shown in Fig. 9. Horizontal and vertical bars indicate the uncertainty associated with each measurement; when not visible, they are smaller than the symbol. The velocity reported at $x = 0$ is the average peak velocity measured exiting from fast flow paths (Table 1).

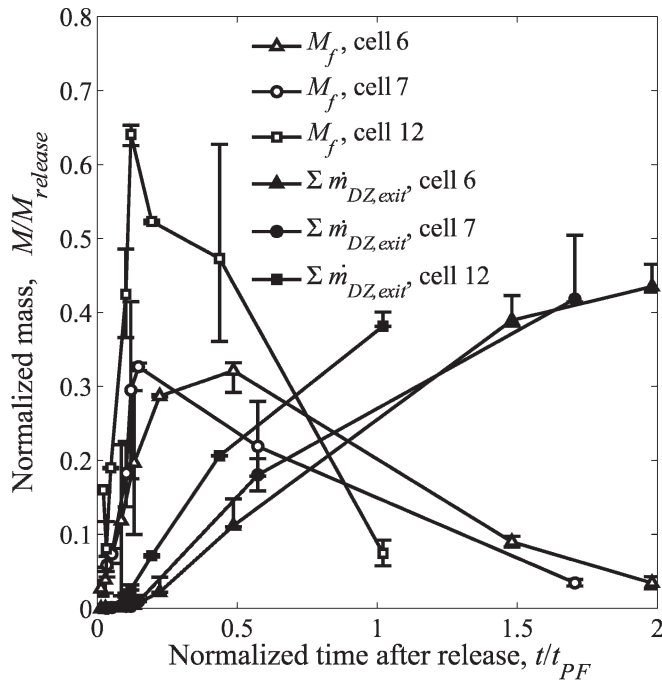


Fig. 11. Estimates of the mass of recovered tracer within the deep zone for the three studies shown in Fig. 9. The total tracer mass within the deep zone, M_f , is obtained by interpolating the concentration measurements shown in Fig. 9 to completely fill the deep zone. Estimates of the tracer mass leaving the deep zone, $\dot{m}_{DZ,exit}$, are obtained from the average concentration observed at the downstream edge of the deep zone. These estimates are integrated to calculate the mass that has exited at each point in time, $\Sigma \dot{m}_{DZ,exit}$. The x -axis shows time normalized by the expected plug-flow time of transport from the dye release location to the end of the deep zone. The y -axis shows tracer mass normalized by the mass released. Vertical bars indicate uncertainty on the basis of different methods of data interpolation.

background was observed at the downstream end of the cell 6 deep zone a scant $T_{touch} = 5.8$ h after the tracer first entered the deep zone (Fig. 9A), which was less than 20% of the expected advection timescale. Similarly, in cells 7 and 12, the tracer first appeared at the downstream end 5.6 h and 5.3 h after release, which corresponds to $T_{touch} = 5.0$ h and 4.7 h after entering the deep zone, respectively. That the first appearance of tracer at the downstream end of the deep zone occurred long before the advection timescale reflects the influence of longitudinal dispersion within the deep zone.

At $t_{PF}/2$ after release, by definition, all of the tracer within the deep zone had traveled through the marsh area in less than the plug-flow time of transit. The total mass of dye within the deep zone at this point in time, M_f , was 20% \pm 9%, 30% \pm 12%, and 42% \pm 6% of what had been released within cells 6, 7, and 12, respectively (Fig. 11, Table 2). These values are an estimate of the fraction of tracer mass that traveled through fast flow paths. Note the excellent agreement in Table 2 between Q_f/Q and M_f/M , both of which are measures of the fraction of flow carried by fast flow paths. Because we expect that dye began to leave the deep zones before the dye that had traveled

through the slow-flow zones entered, it is not surprising that we never observed 100% of the released dye within the deep zone. The mass flux exiting the deep zone, $\dot{m}_{DZ,exit}$, can be estimated from the average concentration at the downstream edge, $C_{DZ,exit}$, by $\dot{m}_{DZ,exit} = C_{DZ,exit}Q$. Figure 11 also shows the integral of this mass flux, which is the cumulative mass that has left the deep zone. The curves are expected to asymptote at $M_{release}$ if the tracer is conservative.

The tracer also spread laterally as it moved through the deep zone. In cell 6 (Fig. 9A), tracer entered the deep zone by 0.6 h after release and had spread across the width of the deep zone by 10.7 h. In cell 7 (Fig. 9B), tracer entered by 1.6 h and had spread across the entire width of the deep zone by 26 h; in cell 12 (Fig. 9C), tracer entered by 1.1 h and had spread across the whole width by 10.1 h. In these three cases the dye mixed across the width of the deep zone on the order of $T_{mix} \approx 10$ h. Because dye entered from multiple fast flow paths, we estimate the lateral length-scale over which the dye mixed as the distance between fast flow paths, $B_c \approx 50\text{--}100$ m. This leads to an estimated lateral dispersivity of $K_y \approx B_c^2/T_{mix} \approx 0.07\text{--}0.3$ m² s⁻¹, or a nondimensional lateral dispersion coefficient of $K_y/u_{PF}B_c = 1\text{--}3$. Similarly, using the transport timescale estimated above for longitudinal dispersivity yields $K_x \approx L_{dz}^2/T_{touch} \approx 0.09\text{--}0.2$ m² s⁻¹, or a nondimensional longitudinal dispersion coefficient of $K_x/u_{PF}L_{dz} = 2\text{--}3$, which agrees well with the estimated lateral dispersion coefficient. Previous work on dispersion in open water suggests that at scales of 50–100 m the horizontal dispersion coefficient falls in the range $K = 0.02\text{--}0.05$ m² s⁻¹ for a patch that is much smaller than the basin (Lawrence et al. 1995). This range is slightly less than the dispersivity we observed here.

Two factors may have contributed to the observed dispersion of tracer: jet entrainment and wind. First, the introduction of fast-flowing water through a confined area can create lateral mixing through shear instabilities. The amount of jet entrainment and hence mixing depends on the excess momentum within the fast-flowing region (Abramovich 1963). However, the rapid decay of the excess velocity and hence momentum (Fig. 10) likely limited the contribution of jet-induced mixing to within 10 m of the upstream edge of the deep zone. Therefore, in this system, it is likely that wind contributed most to the observed mixing. The average wind speed during all releases was $U_{10} = 2.1 \pm 0.2$ m s⁻¹ (cf. Fig. 4). This speed is sufficient to affect transport within an unvegetated area, since surface water speed is approximately 2% of the wind speed at 10 m above the surface (Wetzel 1975), so a 2 m s⁻¹ wind would be expected to advect dye 50 m in less than 1 h. Perhaps most importantly, the deep zone is small enough that the wind can relatively quickly establish basin-scale circulation. For a wind speed $U_{10} = 2.1$ m s⁻¹, the timescale for development of wind-induced circulation across the width of the deep zone would be $B/(0.02U_{10}) \approx 1\text{--}2$ h (George 1981), which is shorter than the observed diurnal wind cycle (Fig. 4) and also less than the observed timescale of longitudinal dye transport across the deep zone (approximately 6 h, cf. Fig. 9). Therefore, basin-scale circulation induced by wind can contribute to mixing.

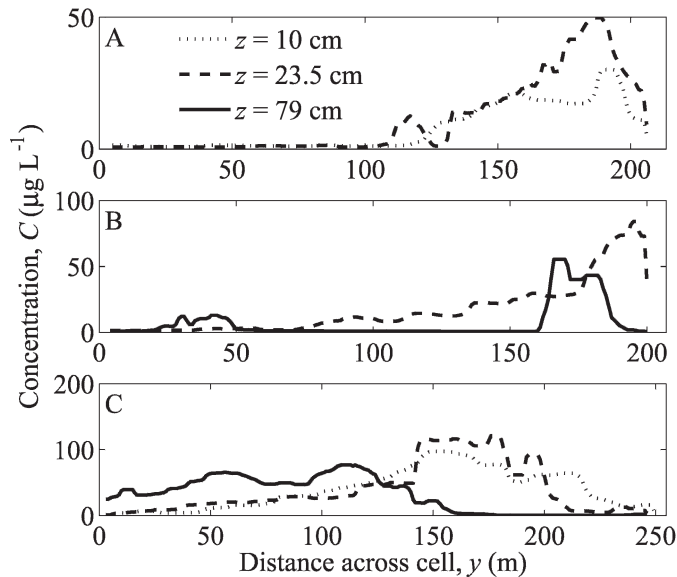


Fig. 12. Dye concentrations at different depths for the three dye releases shown in Fig. 9: (A) cell 6, 6.3 h after tracer release with the wind parallel to flow, (B) cell 7, 5.6 h after release with the wind parallel to flow, and (C) cell 12, 5.3 h after release with the wind perpendicular to flow.

The amount of lateral spreading of the fast-flowing water depended on both the strength and orientation of the local wind. In the first 6 h after the release in cell 6 on 21 July, the wind speed was $U_{10} = 2.9 \pm 0.7 \text{ m s}^{-1}$ oriented parallel to the main flow direction. In the release in cell 7 on 24 July, the wind was $U_{10} = 1.3 \pm 0.4 \text{ m s}^{-1}$, again parallel to the main flow direction though in the opposite direction to the flow. In the release in cell 12 on 26 July, the $3.9 \pm 0.6 \text{ m s}^{-1}$ wind was oriented perpendicular to the main flow direction, so it was directed across the width of the deep zone, blowing from $y = 250 \text{ m}$ toward $y = 0 \text{ m}$. Figure 12 shows the average dye concentrations at different depths between 4.1 and 5.6 h after release for the three dye releases presented in Fig. 9. When the wind was oriented parallel to the direction of flow, we observed mixing over depth but little mixing between water transported within different fast flow paths (Fig. 12A,B). However, wind directed perpendicular to flow enhanced lateral spreading of the dye in a depth-averaged sense (Fig. 12C). In addition, in this release, the wind created distinct patterns of dye concentration over depth. At 5.3 h after release, tracer was observed primarily near the surface ($z = 10 \text{ cm}$) at the downwind edge of the deep zone (near $y = 0 \text{ m}$) and at depth ($z = 79 \text{ cm}$) at the upwind edge (near $y = 250 \text{ m}$). These observations suggest that the wind had created a basin-scale circulation within the deep zone, advecting surface water from west to east, creating a return current near the bottom of the deep zone from east to west. It is clear from these cases that, depending on its orientation relative to the long axis of the deep zone, even a mild wind has the potential to redirect flow. Predictions of the effect of a deep zone on chemical fate within a wetland should therefore consider both windy and nonwindy conditions. For example, the central pond in a southern California wetland providing tertiary treatment for reclaimed water was designed to have

full exposure to prevailing winds to maximize mixing and contaminant removal (Sartoris et al. 2000).

Comparison of temperature within vegetated and unvegetated regions—Temperature loggers were deployed throughout the study period. First, we will consider the loggers located within the open-water deep zones (Fig. 13). These loggers show a typical diel pattern, with a daily minimum in the early morning and a daily maximum in the late afternoon. In general, the temperature fluctuations within the water were not as extreme as they were in the air (Fig. 3C). The composite temperature record shows that, at the surface of the open water, the temperature increased an average of 3.0 ± 0.2 above the nightly minimum (Fig. 14). This thermal variation was damped near the bed, at $z = 60 \text{ cm}$, where temperature only increased to 0.5 ± 0.2 above the daily minimum. The vertical variation in diurnal heating created thermal stratification within the open water during daylight hours. For example, on 10 July, there was a 7.4 ± 0.3 difference between the temperatures 10 cm below the surface and 60 cm below the surface (Fig. 13). Mats of free-floating duckweed (*Lemnaceae*) were present within the open areas and at times were located above the thermistor chains, but all measurements were taken at least 10 cm below these mats. Dale and Gillespie (1976) report that the temperature 2 cm below a duckweed mat can be up to 11°C higher than the temperature within adjacent open water at the same depth. However, at a depth of $z = 10 \text{ cm}$ and below there is little difference between the temperature beneath an open water column and a duckweed cover (Dale and Gillespie 1976).

Now compare the temperature measured within the open water of the deep zones and the temperature measured within the marsh. Temperature fluctuations were reduced within the densely vegetated areas compared with the open area; at its peak, the temperature within dense vegetation remained an average of $2.0^\circ\text{C} \pm 0.3^\circ\text{C}$ cooler than the surface of the open areas. Fast flow paths within the vegetated areas were $0.9^\circ\text{C} \pm 0.3^\circ\text{C}$ warmer than the slow-flow areas, and in some cases their temperature approached that of the surface of the open-water zones (cf. 27 July in Fig. 13). The higher temperature in the fast flow paths was likely caused by advection from the warm temperatures within an upstream open-water area. If the water within the fast flow paths short-circuited the entire marsh region at the same velocity as observed at the exit, then it would have left an upstream open-water deep zone approximately 2–4 h before it entered the deep zone, whereas the water traveling through the slow-flow zone would have spent about 30 h in dense vegetation. Because the timescale for diurnal cooling is approximately 12 h, only the water traveling through the fast flow path would be expected to retain the upstream temperature signature. Note that the observation of a distinct temperature difference between the fast- and slow-moving zones confirms that limited exchange occurred between these two regions.

In addition, the peak temperatures within both the dense vegetation and the deep portions of the open water occurred later in the day than they did at the surface of the open water. As shown in Fig. 14, the maximum temperature at the

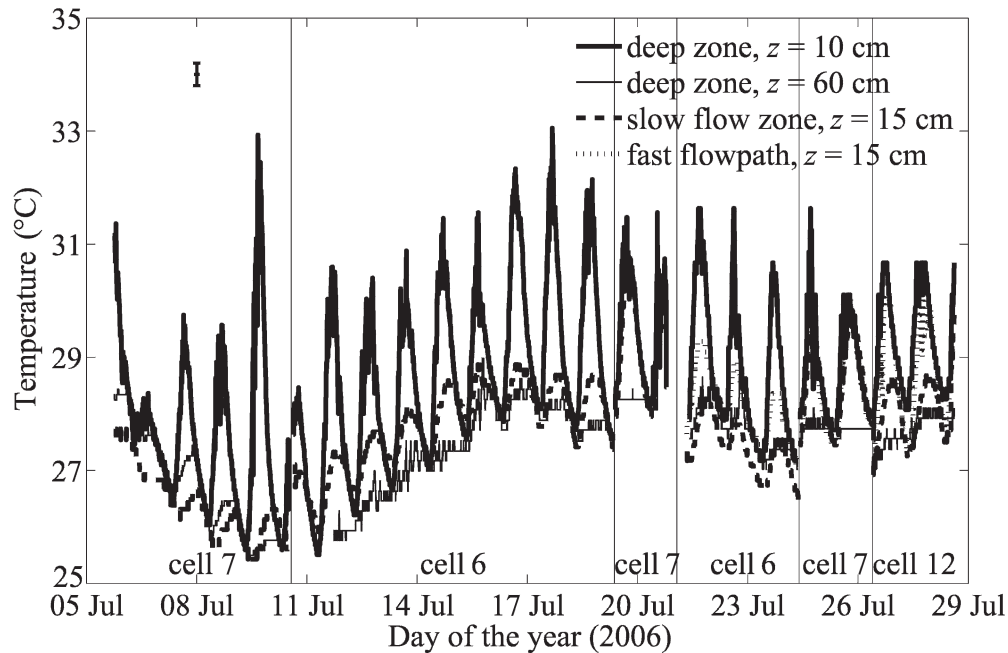


Fig. 13. Temperature recorded by submerged loggers. Solid vertical lines separate deployments in different wetland cells. Within each cell, loggers were placed in up to five different locations: three different depths within the open deep zone (two depths are shown here), 15 cm deep within a densely vegetated region, and 15 cm deep within a fast flow path. The vertical line in the upper left portion of the plot indicates the average expected uncertainty for all lines.

surface of the deep zone occurred at 16:30 h, the maximum temperature 30 cm below the deep zone surface and within the fast flow paths occurred at 18:00 h, and the maximum temperature within the vegetation occurred at 20:00 h. The lag in temperature maxima with depth has elsewhere been attributed to vertical heat transfer from surface to deep waters (Dale and Gillespie 1976).

These observations of spatial and temporal variation in temperature records are consistent with observations elsewhere. For example, Kadlec (2006) reports that the

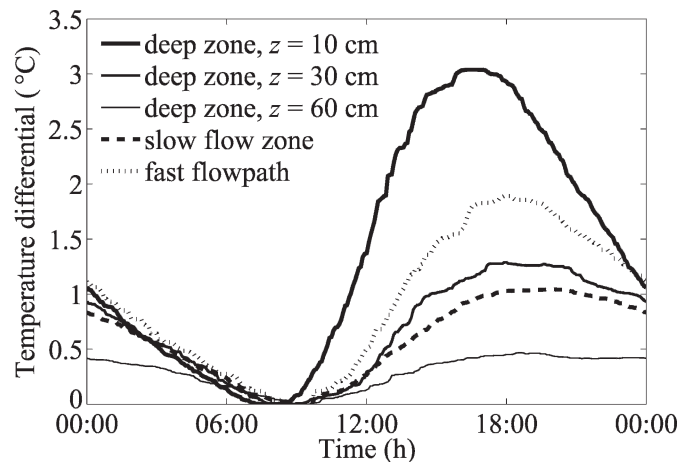


Fig. 14. Composite temperature record from temperature logger data shown in Fig. 13, plus data for loggers within the deep zone 30 cm below the surface. Results are plotted as deviations from the nightly minimum temperature.

water temperature fluctuates diurnally by 6°C within the Hayfield cell in the Tres Rios wetlands, with a daily minimum at 08:00 h and a daily peak at 18:00 h. In a southern California treatment wetland, water temperatures within a band of mixed *Schoenoplectus acutus* and *Schoenoplectus californicus* were up to 2.5°C lower than those within a nearby 12-m-wide open-water area (Sartoris et al. 2000). In the large stormwater treatment areas near the Florida Everglades, temperature variability was reduced in stands of *Typha domingensis* Pers. and *Typha latifolia* L. sp. stands when compared with open water (Chimney et al. 2006). During the growing season, the floating water hyacinth *Eichhornia crassipes* damps temperature fluctuations compared with both the air and with a nearby submerged bed of *Ceratophyllum* (Ultsch 1973).

The horizontal temperature differences that we observed in the Augusta wetland are sufficient to create density-driven exchange flows. For the values we observed in the Augusta wetland, the model presented by Tanino et al. (2005) predicts exchange currents between the vegetation and deep zones with a speed up to 0.9 cm s⁻¹. This flow speed is an order of magnitude larger than the water velocity through the densely vegetated marsh ($U_s < 0.1$ cm s⁻¹) and could result in the exchange of an average of 11 L s⁻¹ between a vegetated region and an adjacent deep zone. It may also contribute flux in the reverse direction from the mean hydraulic gradient, which would enhance dispersion. However, the estimated thermal exchange is approximately 11% of the pumped flow rate through this wetland (100 L s⁻¹), so it probably does not play an important role here. Such convective exchange flows may be important in a natural wetland that lacks an

imposed flow. Oldham and Sturman (2001) observed nightly exchange currents with a velocity of $0.05\text{--}0.2\text{ cm s}^{-1}$ in a constructed wetland mesocosm in Western Australia that had *Schoenoplectus validus* growing in the shallow regions. Within a small midwestern lake, a temperature difference of 2°C between a 1,000-m-long shallow vegetated area and a deeper open-water area was observed to drive a horizontal exchange flow of 0.36 L s^{-1} between the two areas, which constituted a large fraction of overall flux between the two regions (James and Barko 1991).

The difference in temperature between the vegetated and unvegetated portions of the wetland may also be important for other reasons. First, if temperature varies both temporally and spatially throughout the wetland, a single measurement at one location is not representative of the entire wetland. Second, removal rates for contaminants such as nitrate are proportional to the local temperature (Bachand and Horne 2000), so predictions of removal on the basis of the open-water temperature may overestimate removal within the cooler vegetated portions of a wetland. Finally, the different temperatures within the dense vegetation and the fast flow paths suggest that fast flow paths could be identified using thermal remote sensing techniques, such as an infrared thermal image of the wetland or a high-resolution fiber-optic cable, both of which are now able to detect temperature differences of 0.1°C at 1-m spatial resolution (Loheide and Gorelick 2006; Selker et al. 2006). Until such methods have been explored, however, identifying and characterizing specific fast flow paths will continue to require intense focused effort.

Extensions to other wetlands—In this study we presented a detailed investigation of short-circuiting within marsh regions of uniform depth in a large constructed wetland. Discrete fast flow paths were observed in every section of dense vegetation. Within the Augusta wetland, we observed fast flow paths that together accounted for 20–70% of the flow through these cells. The fast flow paths had an average transport velocity $U_f = 1.0 \pm 0.2\text{ cm s}^{-1}$ and the slow zones had a velocity $U_s = 0.06 \pm 0.03\text{ cm s}^{-1}$. The flow paths constituted 2–8% of the width of each marsh area and contained flow traveling 14–20 times as fast as through the densely vegetated slow-flow zones. This degree of spatial velocity variation confirms that uniform flow is a poor approximation to flow through wetlands. Moreover, this heterogeneity complicates the modeling of biogeochemical processes within wetlands and limits our ability to infer full-scale wetland function on the basis of small-scale test wetlands, because the pattern of short-circuiting may be different.

The flat bathymetry, careful planting, multiple inlet and outlet control structures, and controlled flow rate within the Augusta wetland resulted in optimal conditions to create uniform flow within vegetated marsh regions. That nonuniformities were found under such ideal conditions suggests that even stronger flow heterogeneities occur within natural wetlands, which in general exhibit complicated bathymetry, a large diversity of macrophyte species, a dominant flow path leading to a single outlet, and seasonal and storm-driven fluctuations in flow rate (Mitsch and Gosselink 2000). Moreover, many natural wetlands contain a central, deeper,

channelized flow path, which, once formed, will carry fast flows that inhibit sediment accretion and vegetation regrowth, promoting its persistence over time (Cooper 1994; Stern et al. 2001; Perucca et al. 2007). Additional work is necessary to explore the distribution, development, and persistence of small-scale flow patterns that create short-circuiting in a variety of wetland types and locations.

Although short-circuiting complicates the representation of flow in free-surface wetlands, this study suggests that two velocities may be sufficient to describe water movement through a wetland. In the Augusta wetland, there was not a continuous variation in flow velocities; rather, the distribution was binary. Similarly, Keller and Bays (2002) found that the residence time distribution for a short-circuiting 0.81-km^2 wetland in Florida could be fit by assuming that the wetland consisted of only two flow paths of distinct flow speeds. Although a transient storage model would represent the system mathematically, the low lateral mixing observed between fast- and slow-moving vegetated regions suggests that fitting parameters would not reflect actual wetland processes and could not be extrapolated to different systems or different flow rates within the same system (Hart et al. 1999). A stream-tube model is more physically appropriate for the system. Because only two flow velocities are present, a numerical model of flow in a wetland similar to the Augusta system need not consider an infinite number of stream tubes (e.g., Carleton 2002) but may simply consist of a fast and a slow velocity. This study should aid further modeling efforts to represent flow through wetlands accurately.

References

- ABRAMOVICH, G. N. 1963. The theory of turbulent jets. The Massachusetts Institute of Technology Press.
- AREGA, F., AND B. F. SANDERS. 2004. Dispersion model for tidal wetlands. *J. Hydraul. Eng.* **130**: 739–754.
- BACHAND, P. A. M., AND A. J. HORNE. 2000. Denitrification in constructed free-water surface wetlands: II. Effects of vegetation and temperature. *Ecol. Eng.* **14**: 17–32.
- BAYS, J. S., AND R. L. KNIGHT. 2002. Fort Deposit constructed treatment wetlands system: 10-year review, p. 35–44. *In* J. Pries [ed.], Treatment wetlands for water quality improvement: Quebec 2000 Conference Proceedings. Pandora Press.
- BAZANTE, J., AND OTHERS. 2006. Hydrologic measurements and implications for tree island formation within Everglades National Park. *J. Hydrol.* **329**: 606–619.
- BOLSTER, C. H., AND J. E. SAIIERS. 2002. Development and evaluation of a mathematical model for surface-water flow within the Shark River Slough of the Florida Everglades. *J. Hydrol.* **259**: 221–235.
- CAMPAGNA, A. R., AND D. DA MOTTA MARQUES. 2001. The effect of refinery effluent on the aquatic macrophytes *Scirpus californicus*, *Typha subulata*, and *Zizaniopsis bonariensis*. *Water Sci. Technol.* **44**: 493–498.
- CARLETON, J. N. 2002. Damköhler number distributions and constituent removal in treatment wetlands. *Ecol. Eng.* **19**: 233–248.
- CHIMNEY, M. J., L. WENKERT, AND K. C. PIETRO. 2006. Patterns of vertical stratification in a subtropical constructed wetland in south Florida (USA). *Ecol. Eng.* **27**: 322–330.
- COOPER, A. B. 1994. Coupling wetland treatment to land treatment: An innovative method for nitrogen stripping? *Water Sci. Technol.* **29**: 141–149.

- DALE, H., AND T. GILLESPIE. 1976. The influence of floating vascular plants on the diurnal fluctuations of temperature near the water surface in early spring. *Hydrobiology* **49**: 245–256.
- DIERBERG, F. E., J. J. JUSTON, T. A. DEBUSK, K. PIETRO, AND B. GU. 2005. Relationship between hydraulic efficiency and phosphorus removal in a submerged aquatic vegetation-dominated treatment wetland. *Ecol. Eng.* **25**: 9–23.
- EIDSON, G. W., AND O. P. FLITE. 2005. Multi-year research on the use of constructed wetlands for advanced wastewater treatment. *In* K. J. Hatcher [ed.], Proceedings of the 2005 Georgia Water Resources Conference.
- ERIKSSON, P. G. 2001. Interaction effects of flow velocity and oxygen metabolism on nitrification and denitrification in biofilms on submersed macrophytes. *Biogeochemistry* **55**: 29–44.
- FENG, K., AND F. J. MOLZ. 1997. A 2-D, diffusion-based, wetland flow model. *J. Hydrol.* **96**: 230–250.
- FLITE, O. P., III, J. W. MOAK, B. S. METTS, AND G. W. EIDSON. 2006. Constructed wetlands tracer study, Final Report. Tech. Rep. Project No. 90155. Augusta-Richmond County, Southeastern Natural Sciences Academy.
- FOX, A. M., AND W. T. HALLER. 2000. Production and survivorship of the functional stolons of giant cutgrass, *Zizaniopsis miliacea* (Poaceae). *Am. J. Bot.* **87**: 811–818.
- FROSSARD, W., D. ANDREWS, L. E. MOKRY, A. H. PLUMMER, JR., AND J. L. MANCINI. 1996. Use of constructed wetlands for protection of water quality in water supply reservoirs. Tech. Rep. Tech. Report. 807. American Water Works Association Research Foundation.
- GEORGE, D. G. 1981. Wind-induced water movements in the South Basin of Windermere. *Freshwat. Biol.* **11**: 37–60.
- GUARDO, M., AND R. S. TOMASELLO. 1995. Hydrodynamic simulations of a constructed wetland in South Florida. *Water Resour. Bull.* **31**: 687–701.
- HART, D. R., P. J. MULHOLLAND, E. R. MARZOLF, D. L. DEANGELIS, AND S. P. HENDRICKS. 1999. Relationships between hydraulic parameters in a small stream under varying flow and seasonal conditions. *Hydrol. Process.* **13**: 1497–1510.
- HARVEY, J. W., J. E. SAIERS, AND J. T. NEWLIN. 2005. Solute transport and storage mechanisms in wetlands of the Everglades, south Florida. *Water Resour. Res.* **41**: W05009, doi:10.1029/2004WR003507.
- HOPKINSON, C. S., R. L. WETZEL, AND J. W. DAY, JR. 1988. Simulation models of coastal wetland and estuarine systems: Realization of goals, p. 67–97. *In* W. J. Mitsch, M. Straskraba and S. E. Jorgensen [eds.], *Wetland modeling*. Elsevier.
- JADHAV, R. S., AND S. G. BUCHBERGER. 1995. Effects of vegetation on flow through free water surface wetlands. *Ecol. Eng.* **5**: 481–496.
- JAMES, W. F., AND J. W. BARKO. 1991. Estimation of phosphorus exchange between littoral and pelagic zones during nighttime convective circulation. *Limnol. Oceanogr.* **36**: 179–187.
- KADLEC, R. H. 2006. Water temperature and evapotranspiration in surface flow wetlands in hot arid climate. *Ecol. Eng.* **26**: 328–340.
- , AND R. L. KNIGHT. 1996. *Treatment wetlands*. CRC Press.
- KEEFE, S. H., L. B. BARBER, R. L. RUNKEL, J. N. RYAN, D. M. MCKNIGHT, AND R. D. WASS. 2004. Conservative and reactive solute transport in constructed wetlands. *Water Resour. Res.* **40**: W01201, doi:10.1029/2003WR002130.
- KELLER, C. H., AND J. S. BAYS. 2002. Tracer studies for treatment wetlands, p. 173–181. *In* J. Pries [ed.], *Treatment wetlands for water quality improvement: Quebec 2000 Conference Proceedings*. Pandora Press.
- KJELLIN, J., A. WÖRMAN, H. JOHANSSON, AND A. LINDAHL. 2007. Controlling factors for water residence time and flow patterns in Ekeby treatment wetland, Sweden. *Adv. Water Resour.* **30**: 838–850.
- LAWRENCE, G. A., K. I. ASHLEY, I. N. YONEMITSU, AND J. R. ELLIS. 1995. Natural dispersion in a small lake. *Limnol. Oceanogr.* **40**: 1519–1526.
- LIN, A. Y.-C., J.-F. DEBROUX, J. A. CUNNINGHAM, AND M. REINHARD. 2003. Comparison of rhodamine WT and bromide in the determination of hydraulic characteristics of constructed wetlands. *Ecol. Eng.* **20**: 75–88, doi:10.1016/S0925-8574(03)00005-3.
- LOHEIDE, S. P., II, AND S. M. GORELICK. 2006. Quantifying stream-aquifer interactions through the analysis of remotely sensed thermographic profiles and in situ temperature histories. *Environ. Sci. Technol.* **40**: 3336–3341.
- MARANI, M., S. SILVESTRI, E. BELLUCO, N. URSINO, A. COMERLATI, O. TOSATTO, AND M. PUTTI. 2006. Spatial organization and ecohydrological interactions in oxygen-limited vegetation ecosystems. *Water Resour. Res.* **42**: W06D06, doi:10.1029/2005WR004582.
- MARTINEZ, C. J., AND W. R. WISE. 2003. Hydraulic analysis of Orlando Easterly Wetland. *J. Environ. Eng.* **129**: 553–560.
- MITSCH, W. J., AND J. G. GOSSELINK. 2000. *Wetlands*, 3rd ed. John Wiley & Sons.
- NUNGESSER, M. K., AND M. J. CHIMNEY. 2006. A hydrologic assessment of the Everglades Nutrient Removal Project, a subtropical constructed wetland in South Florida (USA). *Ecol. Eng.* **27**: 331–344.
- OLDHAM, C. E., AND J. J. STURMAN. 2001. The effect of emergent vegetation on convective flushing in shallow wetlands: Scaling and experiments. *Limnol. Oceanogr.* **46**: 1486–1493.
- PERSSON, J. 2005. The use of design elements in wetlands. *Nor. Hydrol.* **36**: 113–120.
- PERUCCA, E., C. CAMPOREALE, AND L. RIDOLFI. 2007. Significance of the riparian vegetation dynamics on meandering river morphodynamics. *Water Resour. Res.* **43**: W03430, doi:10.1029/2006WR005234.
- SARTORIS, J. J., J. S. THULLEN, L. B. BARBER, AND D. E. SALAS. 2000. Investigation of nitrogen transformations in a southern California constructed wastewater treatment wetland. *Ecol. Eng.* **14**: 49–65.
- SELKER, J. S., AND OTHERS. 2006. Distributed fiber-optic temperature sensing for hydrologic systems. *Water Resour. Res.* **42**: W12202, doi:10.1029/2006WR005326.
- STERN, D. A., R. KHANBILVARDI, J. C. ALAIR, AND W. RICHARDSON. 2001. Description of flow through a natural wetland using dye tracer tests. *Ecol. Eng.* **18**: 173–184.
- SU, X., AND C. W. LI. 2002. Large eddy simulation of free surface turbulent flow in partly vegetated open channels. *Int. J. Numer. Meth. Fluids* **39**: 919–937, doi:10.1002/fld.352.
- TANINO, Y., H. M. NEPF, AND P. S. KULIS. 2005. Gravity currents in aquatic canopies. *Water Resour. Res.* **41**: W12402, doi:10.1029/2005WR004216.
- ULTSCH, G. 1973. The effect of water hyacinth (*Eichhornia crassipes*) on the microenvironment of aquatic communities. *Arch. Hydrobiol.* **72**: 460–473.
- WALKER, D. J. 1998. Modelling residence time in stormwater ponds. *Ecol. Eng.* **10**: 247–262.
- WETZEL, R. G. 1975. *Limnology*. W. B. Saunders.
- WÖRMAN, A., AND V. KRONNÄS. 2005. Effect of pond shape and vegetation heterogeneity on flow and treatment performance of constructed wetlands. *J. Hydrol.* **301**: 123–128.

Received: 29 May 2007

Accepted: 6 December 2007

Amended: 7 January 2008